Chapter 9
Dynamic Characteristics of a PEM-FC/ Woody Biomass Engine Hybrid Micro-grid

9.1 Introduction

If the micro-grid is introduced into an urban area, it will be expected that the energy cost of a distributed power supply and emission of greenhouse gas can be reduced. To date, authors have investigated the operating method that connects distributed proton exchange membrane fuel cells (PEM-FC) in a power network and cooperates with it [41, 59]. Although the generation efficiency of a PEM is high, greenhouse gas discharges by the reforming reaction of city gas. On the other hand, micro-combined heat and power (micro-CHP) using a small-scale Stirling engine generator (SEG) has been examined in the UK as an energy system for individual houses [60, 61]. By using woody biomass so that carbon dioxide may circulate, the greenhouse gas amount of emission of a power generation system can be decreased. Therefore, the introduction of SEG using woody biomass is effective in emission control of greenhouse gas [62–64]. However, compared with an internal combustion engine or a fuel cell, the generation efficiency, volume efficiency, equipment cost, etc. of the conventional SEG are small. The energy supply system using the micro-grid can reduce equipment cost compared with the method of introducing generating equipment into each house. Moreover, the energy equipment linked to the micro-grid can help, for example to minimize the amount of greenhouse gas emission. Thus, in this chapter, the dynamic characteristics of the power of the independent micro-grid using hybrid cogeneration (PWHC) of PEM-FC and SEG using woody biomass are investigated. The control response characteristic of SEG depends on the engine structure, the configuration of the combustion chamber, the heat transmission characteristic of the heat source, etc. Until now, optimization of the combustion chamber configuration and the heat transmission characteristic of combustion gas have been investigated [65, 66]. Commonly, the power demand pattern of a house or an apartment house consists of many peaks changed for a short time. Since such a power load is followed, a rapid control response characteristic is required of the generating equip-

S. Obara, *Fuel Cell Micro-grids*,

ment. In order to manage the power quality of the micro-grid, it is necessary to clarify the dynamic characteristics of the power with load fluctuation. So, in this chapter, the dynamic characteristics of the PWHC micro-grid are clarified by a numerical analysis using the results of an investigation of the SEG test machine and PEM-FC.

9.2 System Scheme

9.2.1 The Hybrid Micro-grid

Figure 9.1 shows the model of the independent micro-grid that introduces two-set PWHC (PWHC (1) in House (1), and PWHC (2) in House (5)). The micro-grid of this model consists of eight buildings of House (1) to House (8). The heat supply of the exhaust heat of PWHC, a heat storage tank, and a boiler is separated into the group of House (1) to House (4), and the group of House (5) to House (8). The power of two-set PWHC is supplied to each building through the power grid. The system interconnection device is installed in the contact point of PWHC and a power grid. Moreover, the power of PWHC is changed into 100 V and 50 Hz with an inverter. On the other hand, the exhaust heat of PWHC, the heat of a heat storage tank, and a boiler is supplied to each building through hot water piping (1) and (2). However, this study is limited to the dynamic characteristics of the power for the micro-grid.

Figure 9.2 shows the energy flow and chemical reaction of each component of the proposed system. Chip fuel is supplied to a woody biomass engine (SEG), and power is transmitted to an alternating current synchronous power generator. The heat output of SEG is the high-temperature exhaust gas of the combustion cham-

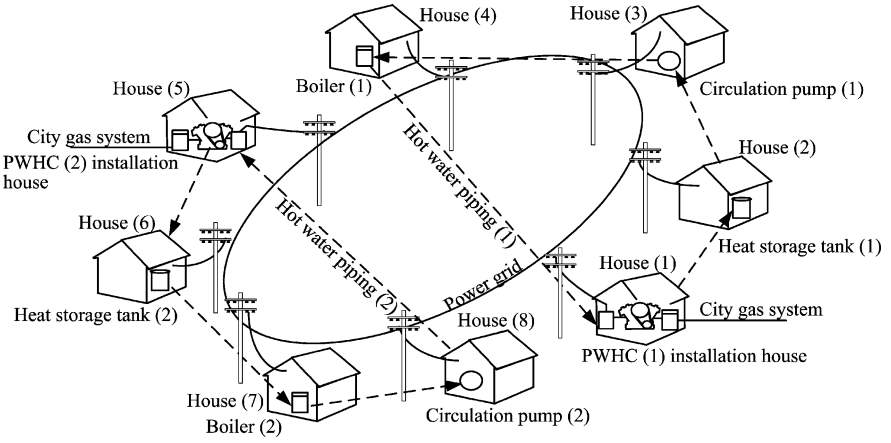

Fig. 9.1 Independent hybrid micro-grid model with PEM-FC and a woody biomass engine

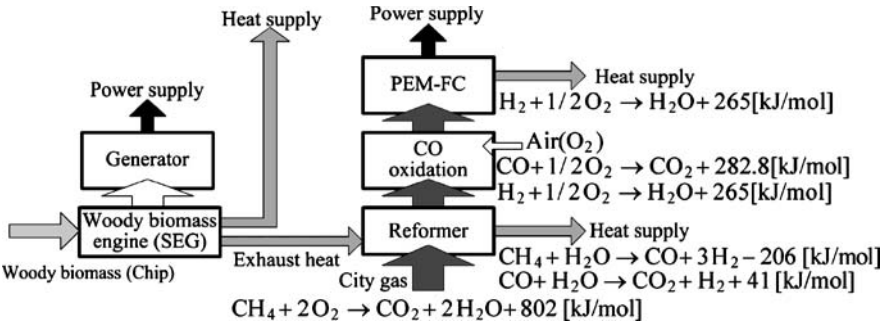

Fig. 9.2 The PWHC power supply system

ber, and engine-cooling hot water. Moreover, as the heat output of PEM-FC, there is fuel cell stack exhaust heat and reformer exhaust heat. In the proposed system, the combustion chamber high-temperature exhaust gas of SEG is supplied to the heat exchanger of the reformer. With a catalyst in the reformer, city gas is changed into reformed gas with a high hydrogen concentration with a reaction temperature of 970 K to 1070 K using this exhaust heat. Reformer exhaust heat is the remaining heat after providing heat to the catalyst through the heat exchanger. In the case study, exhaust heat that can be supplied to the demand side is taken as the reformer exhaust heat and SEG cooling water. Moreover, the demand side is supplied after changing the power of SEG and PEM-FC into an alternating current of constant frequency.

Outline of SEG Testing

Tables 9.1 and 9.2 show the operating conditions and specifications of SEG and the power generator that are examined in this chapter. Although the maximum output of SEG is 3.7 kW, the maximum power load examined according to restric-

Table 9.1 SEG specifications

Engine maximum output	3.7 kW
Test power	1.6 kW
Test number of revolutions	500-550 RPM
Examine heat-medium pressure	0.3 MPa
Number of cylinders	Single cylinder

Table 9.2 Power generator specifications

Maximum output	3 kW
Nominal speed	2700 RPM
Voltage and current	110V, 27.3A
Frequency	180 Hz

tions of the combustion chamber capacity, etc., is 1.6 kW. Figure 9.3 shows a general view of the test equipment. Chip fuel (woody biomass) is fed into the hopper of the combustion chamber. Chips are mixed with preheated air before entering the combustion chamber. The rate of feed of chip fuel is controllable by the fuel feed system installed in the lower part of the hopper. Power is transmitted to the power generator shown in Table 9.2 by a belt from the power shaft of SEG. Since the test SEG is a single cylinder, its vibration is large. Consequently, the combustion chamber is connected with the engine by a buffer duct so that the vibration of the engine does not spread to the combustion chamber. The exhaust gas of the combustion chamber is discharged from the system through a duct. The quantity of heat of the exhaust gas Q_{Ex} and cooling water Q_{Ey} is obtained from the value of the temperature sensor and the flow meter by calculating the transport volume of enthalpy. Moreover, the amount of heat radiation on the combustion chamber surface (Q_{Ez}) is measured by heat flow rate sensor q, and the heat-medium pressure is measured using sensor P_g.

Figure 9.4 shows the experimental results of the energy flow of the test SEG. The energy flow is separated into auxiliary machinery loss, cooling water quantity of heat, exhaust gas quantity of heat, production of electricity, and other losses.

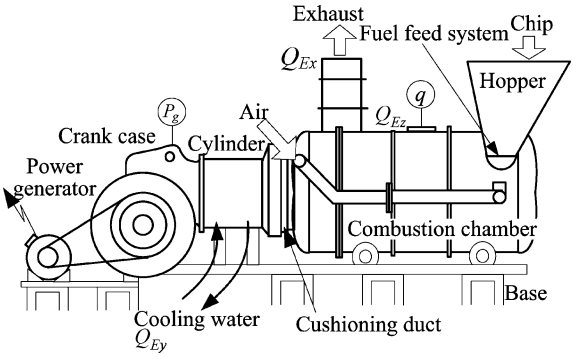

Fig. 9.3 The test woody biomass engine (SEG)

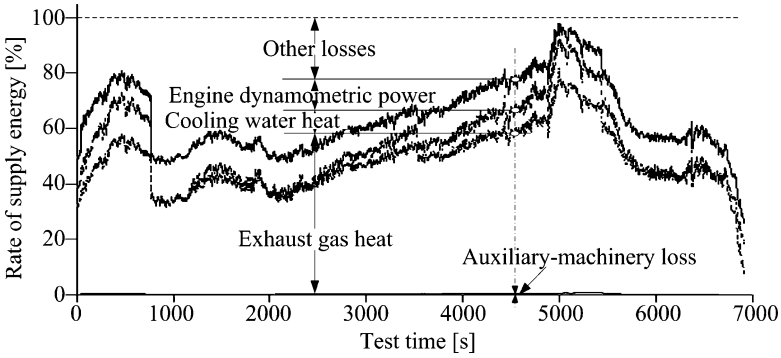

Fig. 9.4 Examination results of SEG energy flow

Other losses of the energy flow are mechanical loss of radiation of heat and friction of SEG, vibration, etc. Other losses decrease, so that the production of electricity of SEG is large. The power generation efficiency of SEG improves by reducing other losses that hold a large part of the energy flow at the time of low load. The quantity of exhaust gas heat holds the largest part in the energy flow, and it is always large compared to the cooling water quantity of heat. Since there is large exhaust gas heat, the development of a compound cycle of operating a steam turbine using the high-temperature exhaust gas of SEG, for example, is possible. Auxiliary machinery loss holds very few parts in the whole energy flow.

9.2.2 The Micro-grid System Operating Method

Figure 9.5 shows the PWHC operation model on a representation day. In this operation pattern, SEG is operated in a range smaller than the base load set up beforehand. In addition to SEG, PEM-FC is operated in a larger load range than the base load. When a load exceeds the base load, SEG can be operated at a maximum efficiency point. However, when a load is less than the base load, a load following operation is required of SEG.

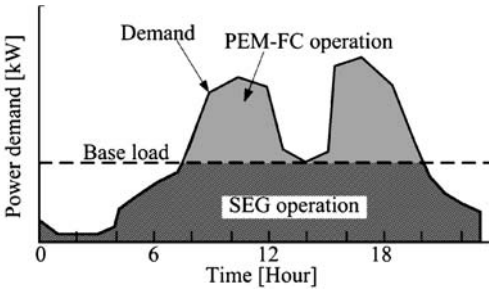

Fig. 9.5 The PWHC operation model

9.3 Control Response Characteristics of PEM-FC and SEG

9.3.1 The Control Block Diagram

Figures 9.6(a) and (b) are the block diagram of the feedback control on the micro-grid by SEG and PEM-FC, respectively. Proportional-plus-integral control (PI control) is introduced into the control of each system. PEM-FC and SEG are controlled by the controller. Each controller is controlled based on the PI control parameters (P and I) set up beforehand. The power generated by SEG and PEM-FC is supplied to the demand side through an inverter and a system interconnection device. The transfer functions of each equipment shown in Figs. 9.6(a) and

(b) describe the determination method in the sections "Response Characteristics of PEM-FC" and "Response Characteristics of SEG".

The control block diagram in the case of one-set SEG operating corresponding to a base load, and corresponding to the load exceeding the base load by one-set PEM-FC is shown in Fig. 9.6(c). SEG supplies the power to the load below the

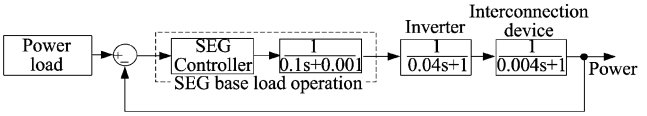

(a) SEG micro grid

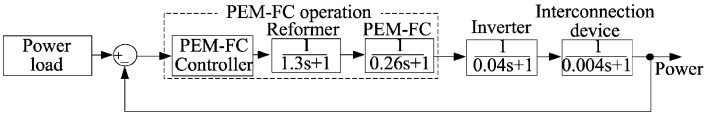

(b) PEM-FC micro grid

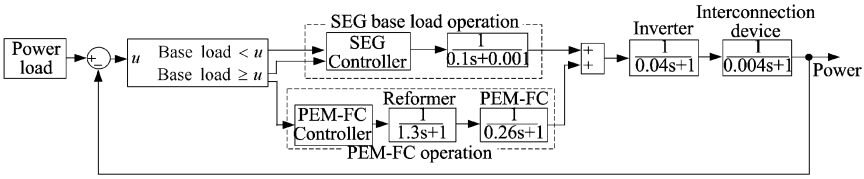

(c) PWHC micro grid with base load operation of SEG

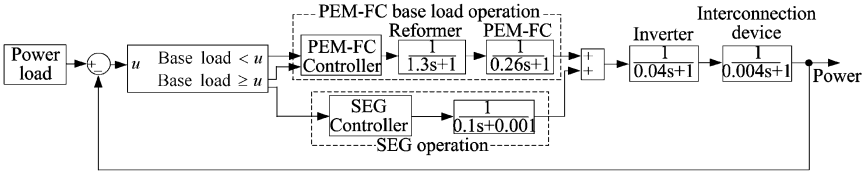

(d) PWHC micro grid with base load operation of PEM-FC

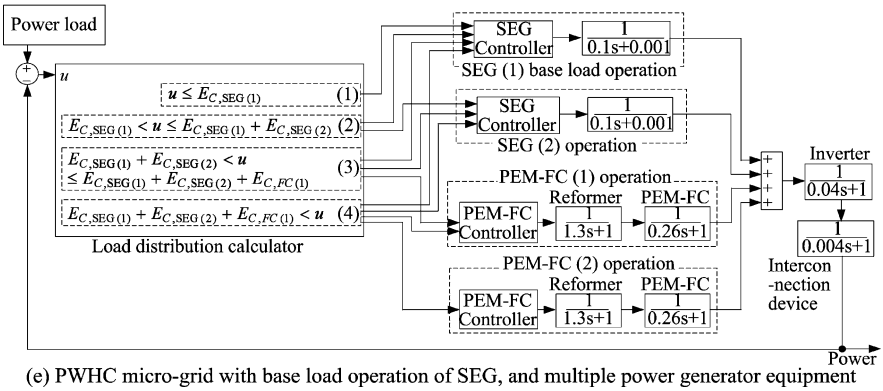

(e) PWHC micro-grid with base load operation of SEG, and multiple power generator equipment

Fig. 9.6 Control block diagram of power supply

base load set up beforehand. PEM-FC is also operated when the load of the micro-grid exceeds the base load. The control block diagram in the case of one-set PEM-FC operating corresponding to the base load, and corresponding to the load exceeding the base load by one-set SEG is shown in Fig. 9.6(d).

The control block diagram of the PWHC micro-grid in the case of one-set SEG operation corresponding to the base load, and corresponding to the load exceeding the base load with multiple generators is shown in Fig. 9.6(e). In Fig. 9.6(e), SEG (1) operates corresponding to the base load, and operates SEG (2), PEM-FC (1), and PEM-FC (2) according to the magnitude of a load. When supplying power to the micro-grid from the combined cycle system, the dynamic characteristics of the micro-grid are determined with the transfer functions of each piece of equipment. So, in this chapter, the transfer function and control parameters of PEM-FC, SEG, an inverter, and a system interconnection device in Fig. 9.6 are determined by the method described in the sections "Response Characteristics of PEM-FC" and "Response Characteristics of SEG".

The transient response characteristics of the power output of the SEG, PEM-FC, the auxiliary machine, and the PWHC micro-grid have been analyzed by MATLAB® (Ver.7.0)/Simulink® (Ver.6.0) of The MathWorks Corporation. In the solver to be used, the Runge–Kutta method is installed, and the sampling time of analysis is calculated automatically and determined so that error may be less than 0.1%.

9.3.2 Response Characteristics of PEM-FC

Table 9.3 shows the result of the investigation of the transfer function in the previous study about the fuel cell stack, the reformer, the inverter, and the system interconnection device [57, 64]. The transfer function of the fuel cell stack was determined from the experimental result, and the transfer function of other equipment was decided from references [27, 47–51, 67, 68]. In the further last study, the optimal value of the parameters of the PI control introduced into the controller of PEM-FC was also investigated. The transfer function and control parameters on the PEM-FC of the control block diagram shown in Fig. 9.6 introduce each value of Table 9.3.

Table 9.3 The transfer function of a power output

Equipment	Transfer function of first-order
Fuel cell stack	Input → $\frac{1}{0.26s+1}$ → Output
Reformer	Input (Fuel) → $\frac{1}{1.3s+1}$ → Output (Reformed gas)
Inverter with DC-AC converter	Input → $\frac{1}{0.04s+1}$ → Output
Interconnection device	Input → $\frac{1}{0.004s+1}$ → Output

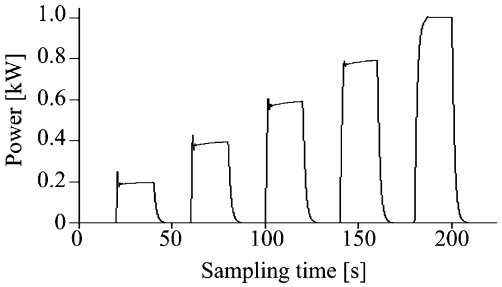

Fig. 9.7 The PI control step response result of the PEM-FC with a reformer ($P = 12.0$, $I = 1.0$)

Figure 9.7 shows the results of the step response of 0.2 kW, 0.4 kW, 0.6 kW, 0.8 kW, 1.0 kW of the PEM-FC with a reformer [57, 64]. In the analysis of Fig. 9.7, the control block diagram of Fig. 9.6(b) was used. The control parameter with a short settling time and small overshooting was investigated by numerical analysis, and P = 12.0 and I = 1.0 were determined. The response time of a system converging on ±5% of a target value is defined as the settling time.

9.3.3 Response Characteristics of SEG

Figure 9.8 shows the experimental result of the step response of 0.2 kW, 0.4 kW, 0.6 kW, 0.8 kW, and 1.0 kW of the testing SEG. As shown in Fig. 9.8, the step response of the testing SEG has large overshooting, and its settling time is long compared with PEM-FC. The heat transmission characteristics between the combustion gas of a chip and the heat exchanger of SEG is considered to influence the settling time greatly. However, it is difficult to improve the rate of heat transfer of the combustion gas of a chip, so that the load fluctuation of the power can be followed. So, in order to shorten the settling time of SEG as much as possible and to reduce overshooting, PI control is added to the operation of SEG.

Figure 9.9 shows the example as a result of a step response obtained in the operating experiment of SEG (Fig. 9.4). The model of the transfer function that simulated this step response is shown in Fig. 9.9. The settling time of the testing SEG exceeds 10 s. Therefore, when SEG is operated so that the fluctuating load

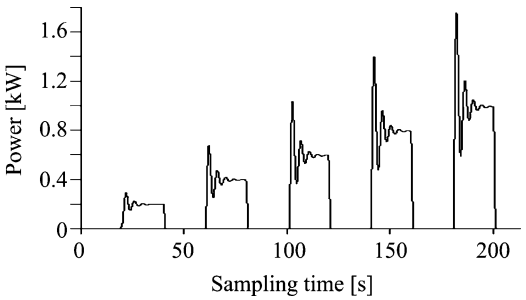

Fig. 9.8 Step response result of SEG when not adding PI control

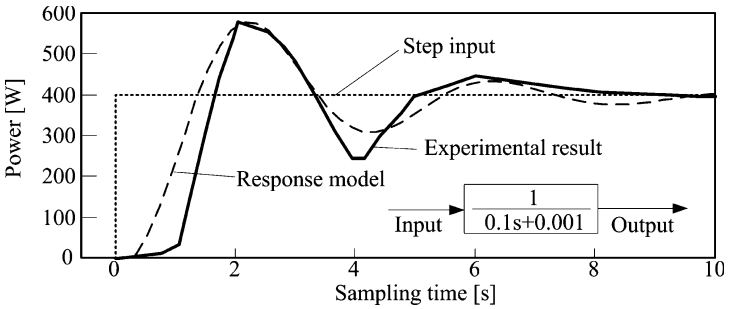

Fig. 9.9 Step response result of the test SEG, and response model

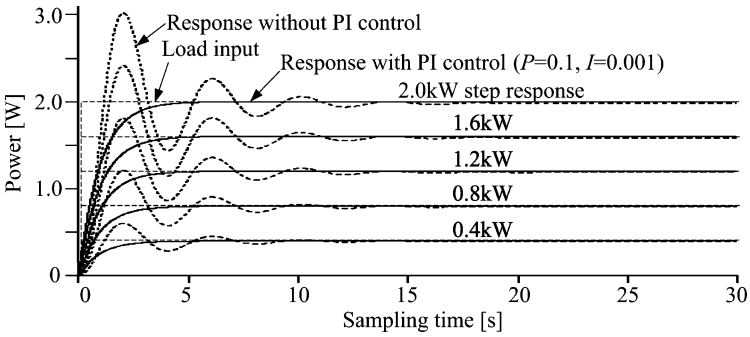

Fig. 9.10 Step response results of 2 kW SEG model

may be followed, the unstable time of voltage and frequency is long. Figure 9.10 shows the analysis results of a step response when adding PI control to the system using the transfer function in Fig. 9.9. The control block diagram used in this analysis is Fig. 9.6(a), and the control parameters of SEG introduced $P = 0.1$ and $I = 0.001$. Moreover, a response result in the case without PI control is also shown in Fig. 9.10. The settling time becomes short by adding PI control to SEG, and an overshoot does not appear. For example, the settling time of the 2 kW step response that does not use PI control is about 16 s. However, if PI control is added, it will improve at about 6 s.

9.4 Results of Dynamic Characteristics Analysis of the PWHC Micro-grid

9.4.1 Power Response Characteristics of PWHC

The 1 kW PWHC micro-grid consists of 0.5 kW SEG and 0.5 kW PEM-FC. Figure 9.11 shows the analysis results of the step response of 0.2 kW, 0.4 kW, 0.6 kW,

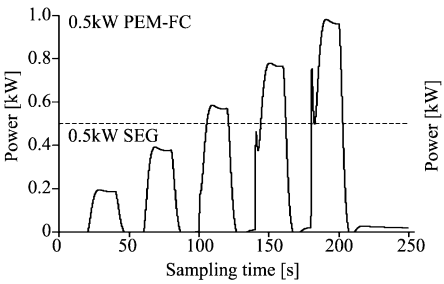

(a) 0.5kW SEG is base-load operation and 0.5kW PEM-FC is load fluctuation operation. PEM-FC of P=12.0 and I=1.0, and SEG of P=0.1 and I=0.001.

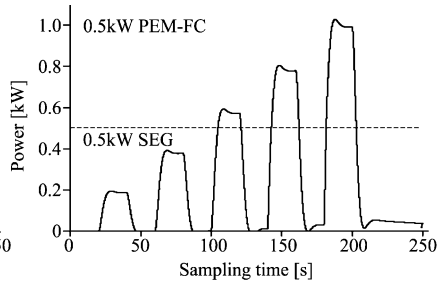

(b) 0.5kW SEG is base-load operation and 0.5kW PEM-FC is load fluctuation operation. PEM-FC of P=0.95 and I=1.1, and SEG of P=0.1 and I=0.001.

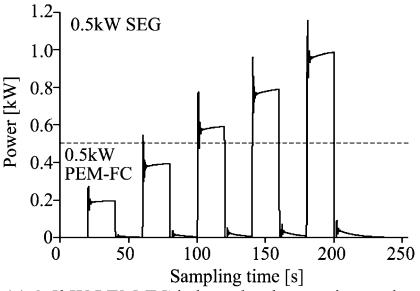

(c) 0.5kW PEM-FC is base-load operation and 0.5kW SEG is load fluctuation operation. PEM-FC of P=12.0 and I=1.0, and SEG of P=0.1 and I=0.001.

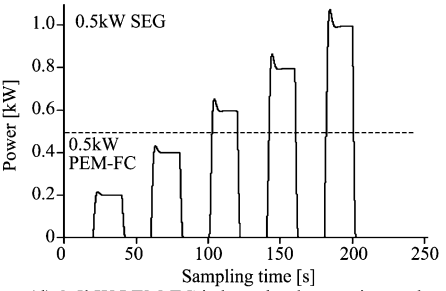

(d) 0.5kW PEM-FC is base-load operation and 0.5kW SEG is load fluctuation operation. PEM-FC of P=0.95 and I=1.1, and SEG of P=0.1 and I=0.001.

Fig. 9.11 Step response result of 1kW PWHC

0.8kW, and 1.0kW of this system. Results in the case when SEG corresponds to the base load and PEM-FC follows the fluctuating load exceeding the base load are shown in Figs. 9.11(a) and (b). The control block diagram used in the analysis in Figs. 9.11(a) and (b) is shown in Fig. 9.6(c). However, the values in Figs. 9.7 ($P = 12.0$ and $I = 1.0$) and 9.10 ($P = 0.1$ and $I = 0.001$) were used for the control parameter of the analysis in Fig. 9.11(a). The speed of response of the PEM-FC shown in Fig. 9.7 is quick compared with the speed of response of SEG shown in Fig. 9.10. From the difference in this speed of response, as shown in the step response of 0.8 kW and 1.0 kW in Fig. 9.11(a), the response of a quick response part and a late response part appears. Consequently, the control parameters of PEM-FC with a quick speed of response are changed, and an improvement of the response characteristics of the PWHC micro-grid is tried. Figure 9.11(b) shows the response characteristics at the time of changing the control parameters of PEM-FC into $P = 0.95$ and $I = 1.1$. These control parameters were decided by trial and error. Two response parts, 0.8 kW and 1.0 kW in Fig. 9.11(a), have improved.

Step response results in the case when PEM-FC corresponds to the base load and SEG follows the fluctuating load exceeding the base load are Figs. 9.11(c) and (d). In the analysis in Figs. 9.11(c) and (d), the control block diagram shown in

Fig. 9.6(d) was used. In Fig. 9.11(c), the control parameters of PEM-FC are $P = 12.0$ and $I = 1.0$, and the control parameters of SEG are $P = 0.1$ and $I = 0.001$. Since the overshoot of the response shown in Fig. 9.11(c) is large, the control parameters of PEM-FC are changed and an improvement is tried. Figure 9.11(d) shows the response characteristics at the time of changing the control parameters of PEM-FC into $P = 0.95$ and $I = 1.1$. These control parameters were determined by trial and error. Compared with the response of Fig. 9.11(c), the response of Fig. 9.11(d) has small overshooting, and its settling time is short.

9.4.2 Response Characteristics of SEG and the PEM-FC Micro-grid Using the Power Load Pattern for Houses

(1) Response Result of SEG

The response characteristics in the case of power supplied to the micro-grid from SEG or PEM-FC are investigated. However, the power load pattern added to the micro-grid assumes two houses on a representative day in February in Sapporo. The power load pattern consists of time average values of the load consumed by the household appliances and electric lights [8]. Space cooling and heating loads are not included in this power load pattern. Therefore, the power load pattern does not have a large difference every month.

Figure 9.12 shows the analysis results of a load response at the time of supplying the power to the micro-grid using 2 kW SEG. The control block diagram used in the analysis of Fig. 9.12 is that of Fig. 9.6(a). Moreover, the control parameters of SEG are $P = 0.1$ and $I = 0.001$ as well as Fig. 9.10. The horizontal axis of Fig. 9.12 is the representative time of analysis. Real time is also displayed on the horizontal axis of Fig. 9.12. Since the calculation time is enormously long, the real-time analysis is performed by shortening the real time to 1/180 in this chapter. Figure 9.12(a) shows the results of a load input and the system response, and Fig. 9.12(b) shows the results of the error of a load input and a response. As for the broken-line part shown in Fig. 9.12(b), the error of the load and the response is over ±5%. A large rising error occurs immediately after 0:00 in Fig. 9.12(b). Actually, since the system is operated continuously, this rising error does not exist. Figure 9.12(c) shows the analysis results of the time period for the error of the load and the response to exceed ±5%. Accordingly, the results of Fig. 9.12(c) express settling times. The settling time when installing SEG into the micro-grid from the result of Fig. 9.12(c) is 10.2 s at the maximum. When the micro-grid is composed from SEG, the unstable period of voltage and a frequency is 10.2 s at the maximum.

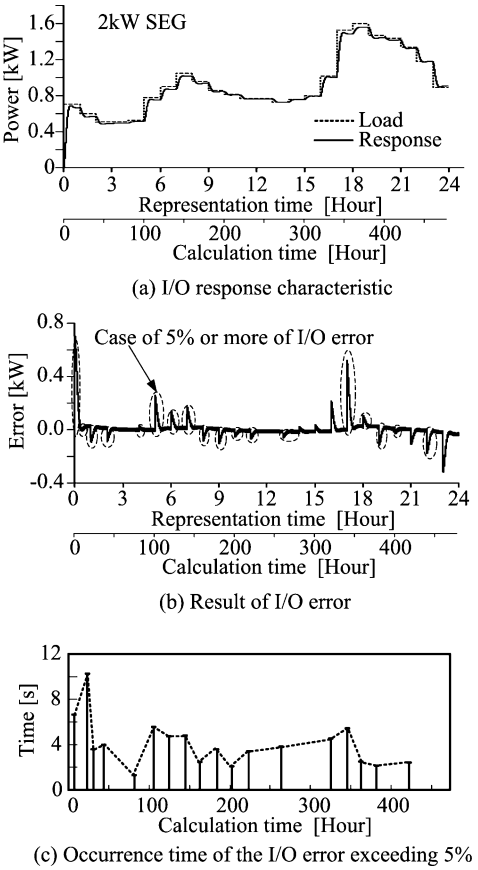

Fig. 9.12 Dynamic characteristics analysis results of the micro-grid at the time of installing the power demand model of two houses in Sapporo. One set of 2 kW SEG. $P = 0.1$ and $I = 0.001$

(2) Response Result of PEM-FC

Figure 9.13 shows the analysis result of a load response at the time of installing 2 kW PEM-FC into the micro-grid. The control block diagram used in the analysis of Fig. 9.13 is that of Fig. 9.6(b). The control parameters set up with the controller are P = 12.0 and I = 1.0, as well as Fig. 9.7. The settling time in the case when PEM-FC composes the micro-grid from the result of Fig. 9.13(c) is 1.6 s or less. However, rising parts are excluded. The power supply due to PEM-FC has a short settling time compared with SEG. Therefore, the dynamic characteristic of the power of the PEM-FC micro-grid is good compared with SEG micro-grid.

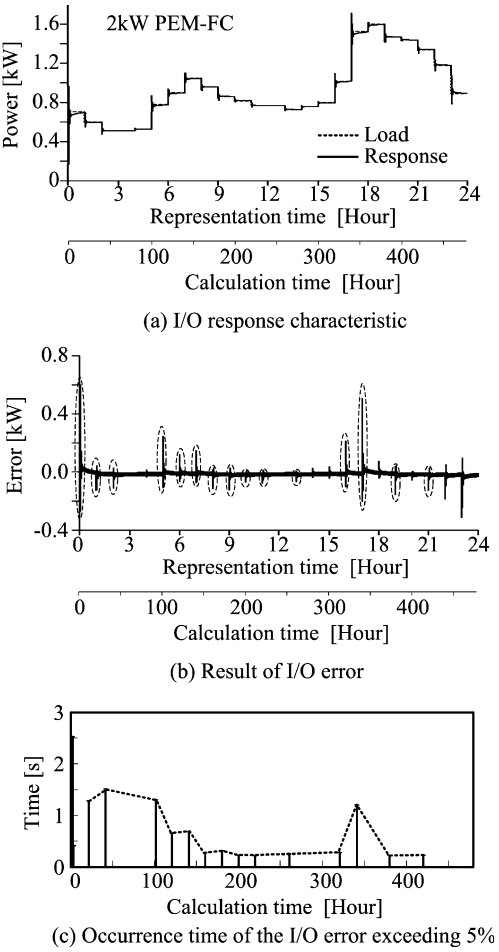

Fig. 9.13 Dynamic characteristics analysis results of the micro-grid at the time of installing the power demand model of two houses in Sapporo. The power is supplied to the grid from 2 kW PEM-FC of one set. PEM-FC of $P = 12.0$ and $I = 1.0$

9.4.3 Response Characteristics of the PWHC Micro-grid Using the Power Load Pattern for Houses

Figure 9.14 shows the analysis results of a load response of the micro-grid composed from 8 kW PWHC. Eight houses are connected to the micro-grid. Woody biomass engine generators installed into the micro-grid are 2 kW SEG (1) and 2 kW SEG (2), in addition 2 kW PEM-FC (1) and 2 kW PEM-FC (2) are installed. Moreover, the control block diagram used in the analysis of Fig. 9.14 is that of Fig. 9.6(e). The control parameters set up with the controller of PEM-FC are $P = 0.95$ and $I = 1.1$ as well as Fig. 9.11(d), and the SEG parameters are $P = 0.1$ and $I = 0.001$. Since the speed of response of SEG is slow, the dynamic characteristics of SEG (2) have a large influence on the micro-grid. It is because SEG (2) is

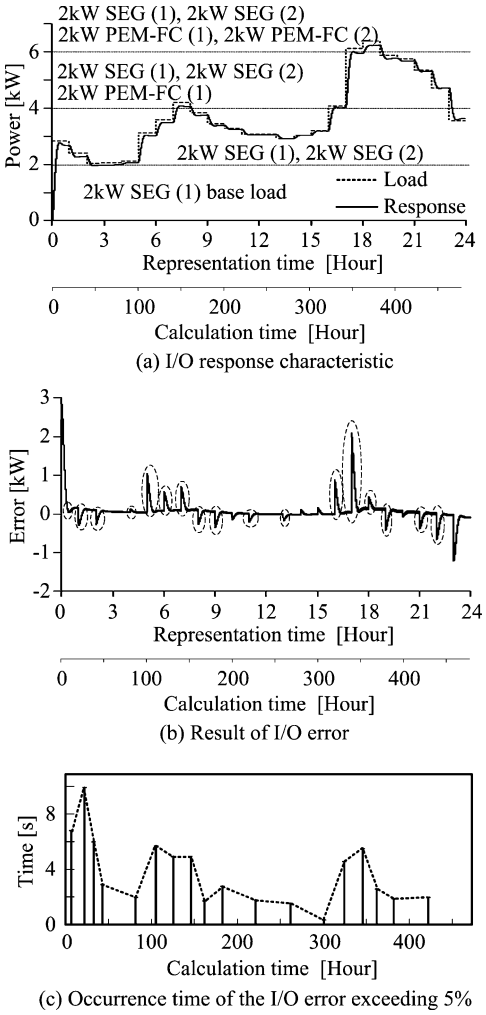

Fig. 9.14 Dynamic characteristics analysis results of the micro-grid at the time of installing the power demand model of eight houses in Sapporo. The power is supplied to the grid from 2 kW SEG of two sets and 2 kW PEM-FC of two sets. PEM-FC of $P = 0.95$ and $I = 1.1$, and SEG of $P = 0.1$ and $I = 0.001$

followed and operated. As a result, the settling time becomes long as shown in Fig. 9.14(c). Consequently, installation of SEG shall be one set corresponding to the base load. With respect to the load exceeding the base load, it corresponds by installing two-set PEM-FC. Figure 9.15 shows the analysis results of the load response of the micro-grid composed from a one-set of 2 kW SEG and a two-set of 2.5 kW PEM-FC. Eight houses are connected to the micro-grid. This system was analyzed by modifying the control block shown in Fig. 9.6(e). The control parameters set up with the controller of PEM-FC are $P = 12.0$ and $I = 1.0$, and the SEG parameters are $P = 0.1$ and $I = 0.001$. The error analysis results in Figs. 9.14(b) and 9.15(b) are similar. However, as shown in Fig. 9.15(c), the settling time of the micro-grid becomes very short compared with that shown

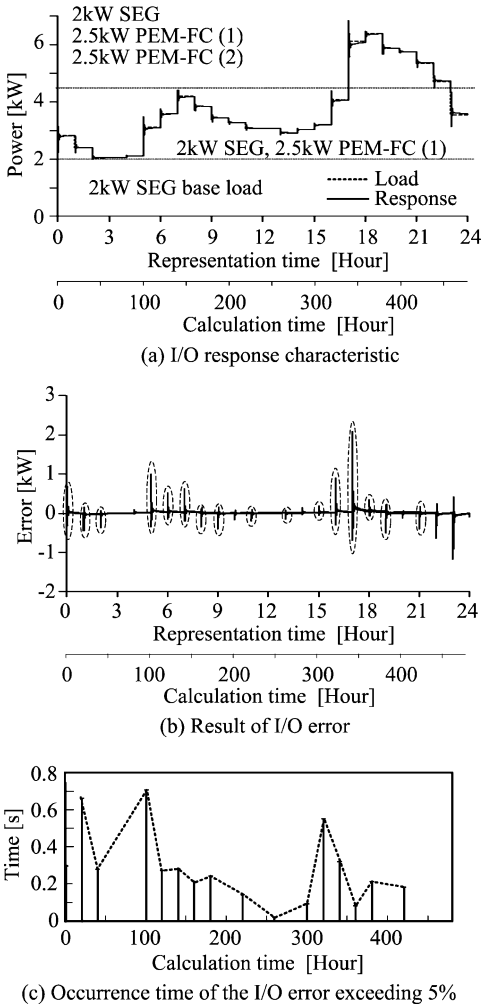

Fig. 9.15 Dynamic characteristics analysis results of the micro-grid at the time of installing the power demand model of eight houses in Sapporo. The power is supplied to the grid from 2 kW SEG of one set and 2.5 kW PEM-FC of two sets. PEM-FC of $P = 12.0$ and $I = 1.0$, and SEG of $P = 0.1$ and $I = 0.001$

in Fig. 9.14(c). The system of Fig. 9.15 is the PWHC micro-grid stabilized dynamically.

9.5 Conclusions

The load response characteristics were investigated using the testing Stirling engine power generator (SEG) that uses woody biomass as a fuel. The transfer function was determined from these results, and the dynamic characteristics of the power of the micro-grid composed from SEG were investigated. Moreover, hybrid cogeneration (PWHC) that uses the combustion exhaust heat of SEG for the heat

source of the reformer of PEM-FC was proposed. The dynamic characteristics of the power when composing the micro-grid from this PWHC were investigated by numerical analysis. Moreover the control parameters installed into each controller of SEG and PEM-FC were examined from the results of numerical analysis. The load response characteristics of the micro-grid using PWHC were investigated, and the following conclusions were obtained.

(1) The settling time of the SEG micro-grid for the power supply to houses exceeds 10 s at the maximum. Therefore, in the SEG independent micro-grid, voltage and frequency may often be instable for a long time.
(2) The micro-grid composed from PEM-FC has a short settling time at the time of load fluctuation compared with the power supply due to SEG. Therefore, the dynamic characteristics of the power of the PEM-FC micro-grid are good compared with SEG.
(3) The micro-grid system that combined the base load operation of SEG and the load following operation of PEM-FC was proposed. The settling time of the proposed micro-grid with eight houses is 1.6 s or less. The micro-grid that installs the proposed system is stable, and there are small amounts of emission of greenhouse gas.

Waveform distortion of a higher harmonic wave (about 10^{-4} to 10^{-2} s), voltage fluctuation (about 10^{-2} to 10^{0} s), frequency change (about 10^{0} to 10^{2} s), and an overvoltage/undervoltage (about 10^{2} s or more) are the dynamic characteristics that should be secured with respect to the power supply of the independent micro-grid. In this chapter, the influence of a period longer than a voltage fluctuation grade (10^{-2} s) was investigated. In addition, the details of the greenhouse gas emission characteristics and the economic evaluation of the proposed system are reported elsewhere [69].